Insights Into Metal−π Arene Interactions of the Highly Lewis Acidic Rh_2^{4+} Core with a Broad Set of π-Ligands: From Ethylene to Corannulene and C_{60}-Fullerene

Andrey Yu. Rogachev and Marina A. Petrukhina*

Department of Chemistry, University at Albany, State University of New York, 1400 Washington Avenue, Albany, New York 12222-0100

Received: February 11, 2009; Revised Manuscript Received: March 23, 2009

The first systematic theoretical investigation of interactions of the Lewis acidic Rh(II) centers with a number of π-ligands having isolated unsaturated carbon−carbon bonds (acetylene and ethylene) or delocalized π-systems with planar (benzene, naphthalene, acenaphthylene, and pyrene) or curved surfaces (corannulene and the C_3-hemifullerene), including the C_{60}-fullerene, has been undertaken. The effect of size, geometry, site specificity, and curvature of π-ligands on their interaction energy with Rh(II) has been examined. The geometric and electronic structures of π-adducts have been modeled at the DFT level of theory by using the hybrid Perdew−Burke−Ernzerhof parameter free exchange−correlation functional (PBE0). The nature of Rh(II)−π interactions was found to be similar in all products with the bonding energy ranging from 14.59 kcal/mol in the benzene adduct to 50.13 kcal/mol in the fullerene complex. Importantly, the quantitative evaluation of two bonding components, namely, ligand-to-metal and metal-to-ligand contributions, allowed us to rationalize the observed trends in π-binding affinity of the selected ligands as well as in stability of the resulting products. These trends deduced from DFT calculations are important for considering the synthetic feasibility of novel π-complexes in these systems.

Introduction

Metal−π interactions have gained general acceptance as important driving forces in supramolecular assembling and molecular recognition processes.[1] This acknowledgment of their significance has considerably improved our understanding of the functioning of biochemical systems such as ion channels, drug receptors, and enzymes.[2] Additionally, the role of transition metal−π interactions has been found relevant for applications in organic synthesis,[3] bond activation,[4] and catalysis.[5] Up to now, numerous theoretical studies have been performed on the cation−π binding of alkali or alkaline earth metal ions.[6] Their focus was devoted to understanding the physical origin of such noncovalent forces and for the quantitative evaluation of their strength. Initially, mainly single-ring arenes and small planar polycyclic aromatic hydrocarbons were used as models. Recently, these studies have incorporated some transition metal ions[7] and extended nonplanar polyaromatic systems.[8] However, to date, only sporadic theoretical studies have been dedicated to modeling the cation−π interactions of heavy transition metals. This remains a very challenging task[9] from the computational viewpoint because of relativistic, spin−orbit coupling and other effects, significantly complicating general applicability of theoretical methods and requiring individual consideration of each transition metal system.

The focus of this study is rhodium(II)−π interactions. Over the years, we have revealed a remarkable reactivity of highly electrophilic dirhodium(II) tetratrifluoroacetate in inorganic,[10] organometallic[11] and supramolecular reactions.[12] Moreover, the applications of the dirhodium core compounds[13] span such diverse areas as catalysis,[14] antitumor metallopharmaceuticals,[15] phototheraupeutic agents,[16] photochemistry,[17] and self-assembly processes.[18] However, no systematic theoretical insight into rhodium(II) binding affinities has been given. Only guanidine interactions with dirhodium tetracarboxylate compounds have recently been studied by quantum chemical methods to unravel mechanisms of their antitumor activity.[19] Therefore, in this work, we set out to broadly investigate interactions of the Rh_2^{4+} core with different types of unsaturated hydrocarbons by using density functional theory (DFT) methods. An account of gas-phase synthesis, X-ray crystallographic characterization, and some properties of a structurally diverse family of the $[Rh_2(O_2CCF_3)_4]$-adducts with aromatic ligands has recently been given,[20] but understanding of bonding in such systems was lacking. Herein, we examine the nature of interactions, binding affinities, and trends in bonding energies of metal−π complexes formed by a very electrophilic Rh_2^{4+} core and axially bound unsaturated hydrocarbons. We gradually change the nature of the latter from systems with isolated multiple carbon−carbon bonds (C_2H_2 and C_2H_4), via cyclic aromatic (C_6H_6) and planar polyaromatic ($C_{10}H_8$, $C_{12}H_8$, and $C_{16}H_{10}$) molecules, to nonplanar open geodesic π-bowls ($C_{20}H_{10}$ and $C_{30}H_{12}$), and finally, to the completely closed C_{60}-ball.

Calculation Details

Geometry Optimization. Full geometry optimization of all adducts was performed at the DFT level by using the hybrid Perdew−Burke−Ernzerhof parameter free exchange−correlation functional (PBE0),[21] which was reported to better describe coordination compounds of heavy transition metals with weak bonding.[22] Also, this functional was successfully applied to model structures and properties of curved polyaromatic systems such as nanotubes and their complexes with metal ions.[23] The Hay-and-Wadt effective core potentials (ECP) and the LANL2DZ[24] basis sets were used for Rh atoms. The standard double-ζ 6-31G(d) basis sets were utilized for all nonmetallic atoms. The D_{2h} point group symmetry was used for modeling of acetylene (C_2H_2), ethylene (C_2H_4), naphthalene ($C_{10}H_8$), and pyrene ($C_{16}H_{10}$). The D_{6h}, C_{2v}, C_{5v}, C_3, I_h, and C_4 point group

* Corresponding author. E-mail: marina@albany.edu.

10.1021/jp901271g CCC: $40.75
Published on Web 04/21/2009

symmetry constraints were imposed for modeling of benzene (C_6H_6), acenaphthylene ($C_{12}H_8$), corannulene ($C_{20}H_{10}$), hemifullerene ($C_{30}H_{12}$), buckminsterfullerene (C_{60}), and $[Rh_2(O_2CCF_3)_4]$, respectively. Theoretical calculations of all $[Rh_2(O_2CCF_3)_4]$-adducts were performed without any symmetry constraints (the C_1 point group symmetry). The gradient norm for the geometry optimization was taken to be 10^{-4}. The true minima on potential energy surfaces (PES) were controlled by calculating the Hessian matrix and, as a consequence, harmonic frequencies. The absence of imaginary frequencies indicated that the true minima were achieved.

Single-Point Calculation. When optimizations were completed, single-point calculations were performed by using the same ECP and the same basis set for Rh atoms and the extended triple-ζ 6-311G(d,p) basis sets for all remaining atoms. The Natural Bond Orbital (NBO)[25] analysis based on single-point calculations has been used for a detailed description of the electronic structures of all compounds. Bond orders quoted in the text are those from the Wiberg formulation[26] (so-called Wiberg bond indexes) incorporated in the NBO analysis. Optimized geometry configurations and molecular orbitals (0.035 au isosurface) are visualized with the help of the ChemCraft program package.[27] All calculations were carried out in the frame of the PC GAMESS/Firefly quantum chemistry program package,[28] which is partially based on the GAMESS-US[29] source code.

The bonding energy for all adducts was estimated by using the following formula: $E(\text{bonding}) = E([Rh_2(O_2CCF_3)_4\cdot(\eta^2\text{-L})]) - E([Rh_2(O_2CCF_3)_4]) - E(\text{L})$, where L is an unsaturated hydrocarbon. These values characterize the total energy of bonding between $[Rh_2(O_2CCF_3)_4]$ and a π-ligand including two Rh—C bonds (η^2-coordination) as well as all possible additional interactions. These data are used for comparative evaluation of thermodynamic stability of the resulting products. Additionally, the influence of the basis set quality on bonding energy has been tested. For selected adducts, two extended basis sets, LANL2TZ and LANL2TZ(f), have been used for Rh. The maximum difference in E(bonding) was found to be no more than 1.11 kcal/mol (~5%). This confirms that the LANL2DZ basis set used in this work is a good compromise between accuracy and computational efforts. An estimation of BSSE (counterpoise technique)[30] has been performed for the Rh—ethylene adduct to give 2.01 kcal/mol. Thus, the basis set superposition error was found to be in the range of the generally accepted accuracy for the DFT methods.

The donor—acceptor interactions are quantified by examining all possible interactions between filled (donor) Lewis-type NBOs and empty (acceptor) non-Lewis NBOs and by evaluating their energetic importance by using the second-order perturbation theory in the NBO basis.[25] Because these interactions lead to the loss of occupancy from localized NBOs of an idealized Lewis structure to empty non-Lewis orbitals (and thus to departures from an idealized Lewis structure description), they are referred to as delocalization corrections to the zeroth-order natural Lewis structure. For each donor NBO (i) and acceptor NBO (j), the stabilization energy, $E^{(2)}$, associated with delocalization $i \rightarrow j$ is estimated as

$$\Delta E_{i\rightarrow j}^{(2)} = -2\frac{\langle\sigma_i|\hat{F}|\sigma_j\rangle^2}{\varepsilon_{j^*} - \varepsilon_i}$$

where $\hat{F}$ is an effective orbital Hamiltonian (Fock or Kohn—Sham operator) and $\varepsilon_i = \langle\sigma_i|\hat{F}|\sigma_i\rangle$ and $\varepsilon_{j^*} = \langle\sigma_{j^*}|\hat{F}|\sigma_{j^*}\rangle$ are orbital energies for donor and acceptor NBOs, respectively. When interpreting the results of such estimations, it should be noted that this approach is only performed at the SCF level of theory (i.e., the Fock or Kohn—Sham operator is analyzed in the basis of the NBO), and only bonding interactions are considered (i.e., antibonding contributions are not covered by the NBO analysis and must be calculated separately). Thus, the simultaneous calculation of bonding and stabilization energies $E^{(2)}$ allows us to estimate the thermodynamic stability as well as both metal-to-ligand (M → L) and ligand-to-metal (L → M) electronic contributions.

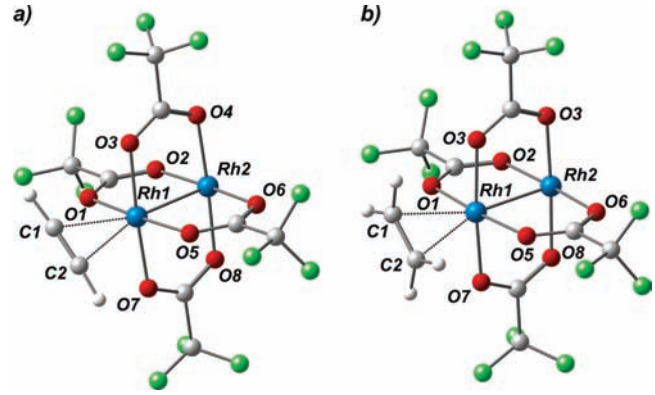

Figure 1. Equilibrium geometry configurations of (a) $[Rh_2(O_2CCF_3)_4\cdot(\eta^2\text{-}C_2H_2)]$ (**1**) and (b) $[Rh_2(O_2CCF_3)_4\cdot(\eta^2\text{-}C_2H_4)]$ (**2**), along with the corresponding labeling schemes.

Results and Discussion

$[Rh_2(O_2CCF_3)_4]$. The orbital model of metal—metal bonding and antibonding interactions within a dimetal core has given chemists a powerful tool to understand structures and reactivity of transition metal dinuclear systems.[13] It has been generally accepted that the formal metal—metal bond order in dirhodium(II,II) tetracarboxylates, $[Rh_2(O_2CR)_4]$, is 1. In a simplified molecular orbital picture of the Rh_2^{4+} core, 8 of the 14 electrons are distributed in the σ-, π-, and δ-orbitals, whereas the remaining 6 electrons occupy the π^*- and δ^*-orbitals, resulting in a ground-state configuration of $\sigma^2\pi^4\delta^2\delta^{*2}\pi^{*4}$ (assuming that the π^* orbitals are destabilized relatively to δ^*). This scheme is supported by a vast amount of structural information reported for various $[Rh_2(O_2CR)_4]$ molecules in which the Rh—Rh bond distances are consistent with a single metal—metal bond.[13] At the same time, the energetic ordering of the Rh—Rh bonding and antibonding orbitals has been under debate for a number of years. Spectroscopic and computational studies have been carried out to understand the electronic structure of various dirhodium systems. The earliest work was done by Dubicki and Martin,[31] who performed extended Hückel calculations on $[Rh_2(O_2CH)_4]$ and concluded that the formal bond order is based on the $\sigma^2\pi^4\delta^2\delta^{*2}\pi^{*4}$ electronic configuration. This report was followed by SCF-Xα calculations for $[Rh_2(O_2CH)_4]$ that indicated the same formal Rh—Rh bond order but suggested that the δ^* orbital is destabilized relative to the π^* level, giving a ground-state configuration of $\sigma^2\pi^4\delta^2\pi^{*4}\delta^{*2}$.[32] The switching of the Rh—Rh π^* and δ^* levels was attributed to the filled—filled symmetry interaction between the δ^* orbital and the appropriate symmetry combination of the oxygen π-type lone pairs. Other relatively high-level theoretical treatments of $[Rh_2(O_2CR)_4]$ have reported different ground-state configurations. For example, ab initio calculations performed by Nakatsuji and co-workers suggested a ground-state configuration of $\pi^4\delta^2\pi^{*4}\delta^{*2}\sigma^2$.[33] More recent SCF-Xα-SW calculations for $[Rh_2(O_2CCF_3)_4]$ concur with the earlier Xα results by suggesting an orbital ordering of

TABLE 1: Selected Calculated Parameters for $[Rh_2(O_2CCF_3)_4]$, C_2H_2, C_2H_4, and Their Adducts, 1 and 2

	compound				
parameter	$[Rh_2(O_2CCF_3)_4]$	C_2H_2	C_2H_4	**1**	**2**
Rh(1)−Rh(2)	2.385			2.412	2.425
Rh(1)−C(1)				2.448	2.416
Rh(1)−C(2)				2.448	2.416
C(1)−C(2)		1.205	1.329	1.217	1.355
order, Rh(1)−Rh(2)	0.799			0.676	0.642
order, C(1)−C(2)		2.993	2.044	2.794	1.780
charge, Rh(1)	+0.966			+0.927	+0.918
charge, Rh(2)	+0.966			+0.895	+0.878
charge, C(1)		−0.229	−0.373	−0.211	−0.378
charge, C(2)		−0.229	−0.373	−0.211	−0.378
$E^{(2)}$(M→L), kcal/mol				7.50	10.94
$E^{(2)}$(L→M), kcal/mol				24.10	37.91
E(bonding), kcal/mol				16.60	20.59

$\sigma^2\pi^4\delta^2\pi^{*4}\delta^{*2}$ with an energy separation between the δ^* and π^* orbitals of 0.48 eV.[34] From the photoelectron spectroscopy point of view augmented by density functional calculations (DFT/BLYP), it can only be concluded that the δ^* and π^* ionization energies are similar within the spread of vibrational energies with excitation (0.2 eV).[35]

Herein, we performed calculations by using the DFT level of theory with the new hybrid parameters free exchange−correlation functional PBE0 that is successfully used for modeling transition metal clusters.[36] Our results support a ground-state configuration of $\sigma^2\pi^4\delta^2\pi^{*4}\delta^{*2}$ for $[Rh_2(O_2CCF_3)_4]$ (Supporting Information, Figure S33). However, the difference between the δ^* and two degenerate π^* orbitals is so small (0.0079 au, 0.21 eV) that these orbitals can be considered as nearly degenerate.

Some important features of the electronic structure of unligated $[Rh_2(O_2CCF_3)_4]$ should be briefly mentioned before discussing its complexation with π-systems. First, the lowest unoccupied molecular orbital (LUMO) lies 0.0523 au (1.42 eV) lower than the next unoccupied molecular orbital (LUMO + 1). This difference in energy, along with symmetry reasons, precludes the possibility to donate electrons into LUMO + 1, and as a result, only LUMO can be considered as an electron acceptor from a donor (aryne, arene, or polyaromatic hydrocarbon molecules). Second, the energy degeneracy of the two π^* and one δ^* orbitals could make all of them suitable for π back-donation. However, the symmetry requirement for the accepting orbital to be of the σ^*-type, which is d_z^2, causes a back-donating orbital to include a z component. This leaves the σ^* orbital as an acceptor and one of the two π^* orbitals as a donor of electrons in respect to the axially bound π-ligands. Importantly, the calculated charges at open rhodium(II) centers in $[Rh_2(O_2CCF_3)_4]$ are 0.966 (Table 1), thus confirming the latter to be an extremely avid Lewis acid.

Adducts with C_2H_2 and C_2H_4. Because there are no experimental crystallographic data available for the acetylene adduct, $[Rh_2(O_2CCF_3)_4\cdot(\eta^2\text{-}C_2H_2)]$ (**1**, Figure 1a), the geometrical parameters of the structurally characterized complex with diphenylacetylene[37] were used for comparison (Supporting Information, Table S11). The calculated equilibrium geometry of $[Rh_2(O_2CCF_3)_4\cdot(\eta^2\text{-}C_2H_4)]$ (**2**, Figure 1b) is in good agreement with the experimental one obtained by single crystal X-ray diffraction (Supporting Infomation, Table S10).[38] The observed differences between the calculated and crystallographic data for **1** and **2** can be attributed to crystal packing forces that are not taken into account in theoretical modeling, incompleteness of the basis sets, and inherent approximation of the DFT method. However, for molecules as large as these adducts consisting of about 100 atoms, the agreement found between the experimental and theoretical values is considered satisfactory.

SCHEME 1: Schematic Representations of the Interacting MOs in (a) $[Rh_2(O_2CCF_3)_4\cdot(\eta^2\text{-}C_2H_2)]$ (1) and (b) $[Rh_2(O_2CCF_3)_4\cdot(\eta^2\text{-}C_2H_4)]$ (2)

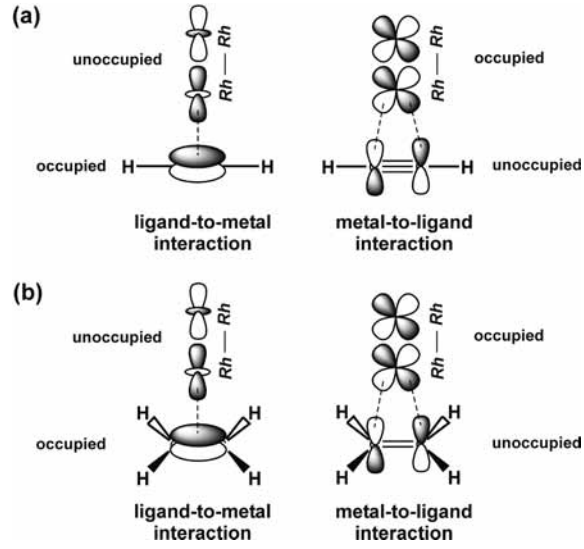

A comparison of the geometrical parameters of **1** and **2** (Table 1) with those of the parent $[Rh_2(O_2CCF_3)_4]$ complex shows that the coordination of both ethylene and acetylene leads to an elongation of the Rh−Rh bond length. This can be explained by (i) an increase in occupancy of antibonding orbitals centered at the Rh_2^{4+} core and (ii) a decrease in occupancy of bonding orbitals localized at the metal−metal bond. Both types of interactions should be important for the dirhodium adducts with π-ligands. The elongation of the C(1)−C(2) bond length of coordinated hydrocarbons in **1** and **2** is also consistent with the L → M electron donation, which is accompanied by a decrease in occupancy of the ligand π-bonding orbitals.

The Rh(1)−C bond lengths are noticeably shorter in **2** (Table 1), indicating a stronger interaction in $[Rh_2(O_2CCF_3)_4\cdot(\eta^2\text{-}C_2H_4)]$ compared to that in $[Rh_2(O_2CCF_3)_4\cdot(\eta^2\text{-}C_2H_2)]$. This is in line with the estimated bonding energies of the corresponding adducts, 20.59 kcal/mol in **2** versus 16.60 kcal/mol in **1**. To follow up on these results, a detailed analysis of the electronic structures of **1** and **2** was carried out in terms of NBO.[25] Specifically, the second-order perturbation theory in the frame of NBO was applied, and that allowed us to decompose interactions between the dimetal unit and hydrocarbons into two components, namely, L → M and M → L contributions (Scheme 1). The L → M interaction mainly corresponds to electron donation from the highest occupied MO (HOMO) of an axial

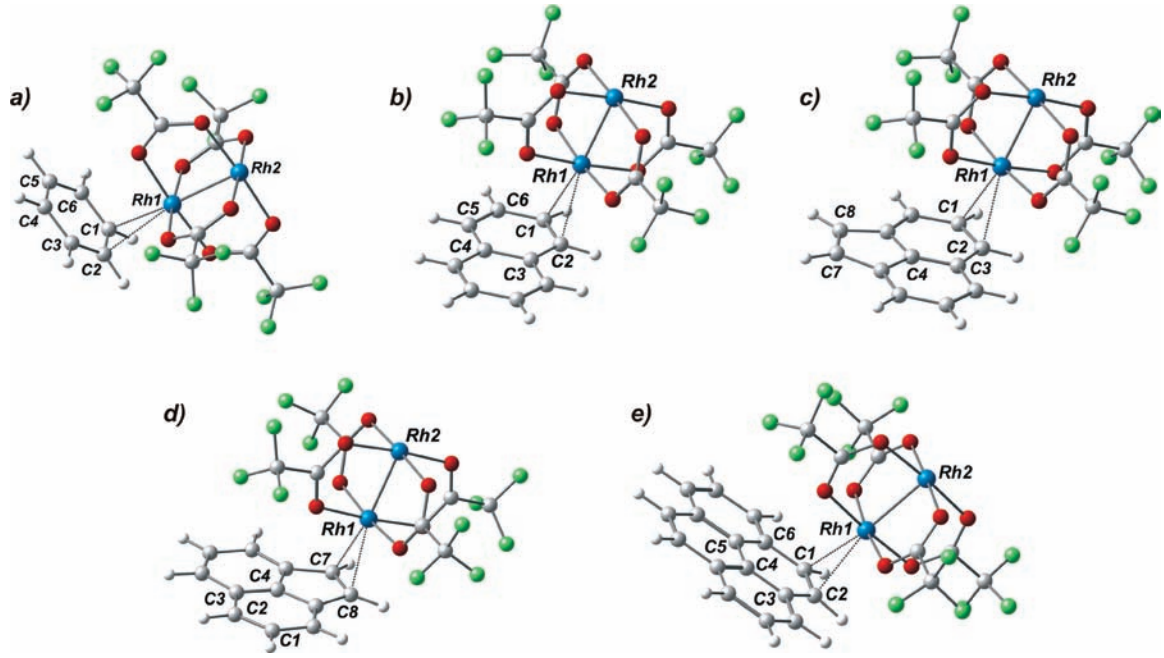

Figure 2. Equilibrium geometry configurations of (a) $[Rh_2(O_2CCF_3)_4 \cdot (\eta^2\text{-}C_6H_6)]$ (**3**), (b) $[Rh_2(O_2CCF_3)_4 \cdot (\eta^2\text{-}rim\text{-}C_{10}H_8)]$ (**4a**), (c) $[Rh_2(O_2CCF_3)_4 \cdot (\eta^2\text{-}rim\text{-}C_{12}H_8)]$ (**5a**), (d) $[Rh_2(O_2CCF_3)_4 \cdot (\eta^2\text{-}hub\text{-}C_{12}H_8)]$ (**5b**), and (e) $[Rh_2(O_2CCF_3)_4 \cdot (\eta^2\text{-}C_{16}H_{10})]$ (**6**), along with the corresponding labeling schemes.

ligand to the σ-type antibonding MO centered at the dimetal core (σ* MO). The M → L interaction mainly involves electron donation from the π-type antibonding molecular orbital (π* MO in accord with Cotton's formulation of metal—metal bonding)[13] centered at the dirhodium core to the lowest unoccupied MO (LUMO) of acetylene or ethylene. It is noteworthy that π* MO of $[Rh_2(O_2CCF_3)_4]$ is not HOMO, but HOMO − 1. HOMO of the dirhodium unit corresponds to δ* MO, which is localized at the dimetal core and is not suitable for interacting with C_2H_2 or C_2H_4 because of symmetry reasons.

The results obtained show that the L → M interactions provide a major contribution to bonding in **1** and **2** (Table 1). Because the σ* antibonding orbital of the dirhodium core is involved in this interaction, a higher value of the L → M interaction energy in **2** leads to a greater decrease of its metal—metal bond order (0.642 and 0.676 in **2** and **1** vs 0.799 in $[Rh_2(O_2CCF_3)_4]$). The nature of L → M interactions is the same in both adducts (Supporting Information, Figures S34 and S35), whereas the difference in energy results from different positioning of HOMO of ethylene and acetylene on the energy scale. HOMO of C_2H_4 lies higher in energy (−0.2867 au) than that of C_2H_2 (−0.3052 au), and that results in the reduced energy gap between frontier orbitals of interacting partners in **2** compared to **1**. The specific feature of bonding between the dirhodium unit and ethylene or acetylene should be noted here. Because the σ-bonding orbital of the Rh_2^{4+} core is also involved in the L → M donation, the overall interaction should be more precisely described as the 4 electrons−3 orbitals one. However, the contribution of the σ-bonding orbital is small.

Adducts with C_6H_6, $C_{10}H_8$, $C_{12}H_8$, and $C_{16}H_{10}$. For the next step, we have moved to modeling the dirhodium adducts with cyclic aromatic (benzene, C_6H_6) and planar polyaromatic (naphthalene, $C_{10}H_8$; acenaphthylene, $C_{12}H_8$; pyrene, $C_{16}H_{10}$) hydrocarbons (Figure 2). It should be mentioned here that the DFT data for the pyrene adduct have recently been used for a direct comparison of the homometallic Rh—Rh and heterobimetallic Bi—Rh π-complexes.[39] An analysis of calculated geometrical parameters of $[Rh_2(O_2CCF_3)_4 \cdot (\eta^2\text{-}C_6H_6)]$ (**3**), $[Rh_2(O_2CCF_3)_4 \cdot (\eta^2\text{-}rim\text{-}C_{10}H_8)]$ (**4a**), $[Rh_2(O_2CCF_3)_4 \cdot (\eta^2\text{-}rim\text{-}C_{12}H_8)]$ (**5a**), $[Rh_2(O_2CCF_3)_4 \cdot (\eta^2\text{-}hub\text{-}C_{12}H_8)]$ (**5b**), and $[Rh_2(O_2CCF_3)_4 \cdot (\eta^2\text{-}C_{16}H_{10})]$ (**6**) shows their good agreement with experimental data[40] (Supporting Information, Tables S12−S14, S16, and S17). For naphthalene and acenaphthylene that can map onto the surface of the C_{60}-fullerene and the $C_{20}H_{10}$-bowl, the C—C bonds were defined as accepted for corannulene (Scheme 2).[41] In naphthalene, two sites (*rim* and *spoke*) are compared, whereas acenaphthylene provides a unique case with all carbon—carbon bond types (*rim*, *hub*, and *spoke*) of a bowl-shaped polyaromatic system existing in a planar environment. The corresponding *spoke*-isomers, for which there are no experimentally isolated complexes known, will be discussed separately.

SCHEME 2

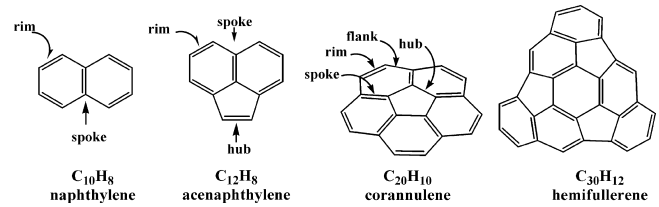

In a series of complexes **3**, **4a**, **5a**, **5b**, and **6** (Table 2), the rhodium—rhodium bond length has the maximum value in the *hub*-isomer with acenaphthylene and then decreases along the row **5b** > **6** > **5a** = **4a** > **3**. This is accompanied by a largest elongation (Δ = 0.032 Å) of the C—C bond directly coordinated to the dimetal unit in **5b** (vs 0.011, 0.017, 0.018, and 0.023 Å in **3**, **4a**, **5a**, and **6**, respectively). Plus, the Rh—C bond lengths are significantly shorter in **5b** compared to those in other adducts with planar polyaromatic ligands. All these tendencies indicate that the metal−π−arene interaction for this series should be the strongest in the *hub*-acenaphthylene complex. This is consistent with the estimated bonding energy values between the dirhodium unit and a polyarene, 23.11 kcal/mol in **5b** versus 14.52, 17.87, 17.74, and 20.08 kcal/mol in **3**, **4a**, **5a**, and **6**, respectively.

A detailed analysis of electronic structures of these adducts in terms of NBO indicates that the L → M contribution is the

TABLE 2: Selected Calculated Parameters for C_6H_6, $C_{10}H_8$, $C_{12}H_8$, $C_{16}H_{10}$, and Their Adducts with $[Rh_2(O_2CCF_3)_4]$, 3−6

	compound										
parameter	C_6H_6	$C_{10}H_8$	$C_{12}H_8$	$C_{16}H_{10}$	**3**	**4a**	**4b**	**5a**	**5b**	**5c**	**6**
Rh(1)−Rh(2)					2.414	2.422	2.406	2.422	2.432	2.421	2.427
Rh(1)−C(1a)[a]					2.591	2.542	2.958	2.534	2.426	2.984	2.487
Rh(1)−C(2a)[a]					2.604	2.575	2.866	2.513	2.428	2.643	2.489
C(1)−C(2)	1.393	1.373	1.381	1.359	1.404	1.390	1.371	1.399	1.384	1.383	1.382
C(3)−C(4)	1.393	1.428	1.393	1.423	1.384	1.423	1.435	1.389	1.396	1.408	1.422
C(7)−C(8)			1.361					1.360	1.393	1.366	
order, Rh(1)−Rh(2)					0.687	0.647	0.736	0.648	0.601	0.677	0.621
order, C(1)−C(2)	1.436	1.555	1.557	1.655	1.394	1.460	1.570	1.460	1.544	1.539	1.506
order, C(3)−C(4)	1.436	1.233	1.280	1.234	1.491	1.244	1.220	1.302	1.263	1.229	1.235
order, C(7)−C(8)			1.746					1.748	1.513	1.689	
charge, Rh(1)					+0.947	+0.936	+0.972	+0.936	+0.927	+0.953	+0.927
charge, Rh(2)					+0.902	+0.883	+0.929	+0.884	+0.855	+0.898	+0.871
charge, C(1)	−0.208	−0.205	−0.209	−0.180	−0.253	−0.229	−0.187	−0.233	−0.206	−0.176	−0.201
charge, C(2)	−0.208	−0.183	−0.167	−0.180	−0.248	−0.222	−0.186	−0.209	−0.147	−0.165	−0.202
charge, C(3)	−0.208	−0.058	−0.065	−0.051	−0.193	−0.060	−0.102	−0.066	−0.067	−0.057	−0.064
charge, C(4)	−0.208	−0.058	−0.052	−0.016	−0.178	−0.048	−0.082	−0.032	−0.021	−0.123	−0.003
charge, C(7)			−0.197					−0.168	−0.204	−0.177	
charge, C(8)			−0.197					−0.203	−0.205	−0.176	
$E^{(2)}$(M → L), kcal/mol					12.34	7.42	4.29	6.46	10.35	4.54	7.97
$E^{(2)}$(L → M), kcal/mol					13.65	38.59	2.71	38.11	51.54	16.03	38.41
E(bonding), kcal/mol					14.52	17.87	9.76	17.74	23.11	13.08	20.08

[a] These carbon atoms are directly bound to a rhodium center. For convenience, in *rim*-isomers, they are designated as C(1) and C(2), in *spoke*-isomers as C(3) and C(4), and in *hub*-isomer as C(7) and C(8).

highest in **5b** and the lowest in the benzene adduct **3** with very similar values found in **4a**, **5a**, and **6**. At the same time, the M → L contribution is even slightly lower in **5b** than that in **3**. Similarly to the above-mentioned adducts with acetylene and ethylene, the main difference in stability is also caused by different L → M energy contributions, although their variation in **1** and **2** was not that drastic. The relative stabilities of all above-mentioned adducts follow the order **5b** > **2** > **6** > **4a** ≈ **5a** > **1** > **3**. By considering this series, it can be generally concluded that extended and conjugated polyaromatic ligands form more stable η^2-adducts than benzene, with the hub-acenaphthylene and ethylene complexes being the most stable.

The nature of M → L and L → M interactions is the same in **3**, **4a**, **5a**, **5b**, and **6** (Scheme 3) and similar to that in the adducts with acetylene (**1**) and ethylene (**2**). The 4 electrons−3 orbitals type of interaction for the M → L electron donation (Supporting Information, Figures S36−S38, S41, and S42) is found in each case. It involves occupied MO of $[Rh_2(O_2CCF_3)_4]$ (HOMO-1, π^* MO) and both unoccupied (LUMO) and occupied MOs of an aromatic ligand, but contribution of the latter is not sufficiently strong. At the same time, the L → M electron donation involves only interaction of HOMO of an arene (except for **5a**, where this orbital is HOMO − 1) with LUMO (σ^* MO mainly localized at the dimetal core) of $[Rh_2(O_2CCF_3)_4]$. Similarly to the acetylene and ethylene adducts, variations in L → M interaction energy can be explained by different positioning of the frontier ligand MOs on the energy scale. Thus, HOMO of acenaphthylene lies higher (−0.2319 au) than the same orbital of benzene (−0.2656 au) and than HOMO − 1 of naphthalene (−0.2444 a.u). One exception involves pyrene which has higher energy of its HOMO (−0.2128 au) compared to $C_{12}H_8$, whereas the stability of the pyrene adduct **6** is lower than that of the acenaphthylene complex **5b**.

It was noticed earlier on the basis of Hückel calculations that the electrophilic dirhodium units tend to coordinate to carbon−carbon bonds of a polyarene having the highest π-bond order.[40b] We have later shown that the direction of this interaction depends on topology of the frontier MO for aromatic ligands.[42] Application of both approaches to the polyarene adducts of $[Rh_2(O_2CCF_3)_4]$ studied here gives the same result. The highest C−C bond order in $C_{12}H_8$ corresponds to the C(7)−C(8) bond (Figure 2d), whereas in naphthalene and pyrene, it is found at the C(1)−C(2) site (Figure 2b,e). Also, suitable HOMO and LUMO of naphthalene and pyrene are localized in a way that their effective interaction with MOs of a dimetal core becomes possible only in the case of the C(1)−C(2) bond (Scheme 3, Supporting Information, Figures S27 and S29). In acenaphthylene, the suitable combination of occupied and unoccupied MOs was found for both C(1)−C(2) and C(7)−(8) sites yielding two stable isomeric adducts (*rim* and *hub*). In contrast, benzene has six equivalent carbon−carbon bonds and exhibits no site preference for η^2-metal coordination (Table 2, Supporting Information, Figure S26). Importantly, the theoretically predicted binding sites of all polyaromatic ligands are consistent with the ones observed experimentally in the structurally characterized dirhodium(II) tetratrifluoroacetate complexes.[40]

***Spoke*-Isomers.** The C_{60}-fullerene is well known to form a variety of stable η^2-exohedral metal complexes[43] in which the metal coordinates to the junction of two six-membered rings corresponding to the so-called *spoke* bond of corannulene.[41] In order to evaluate the reactivity of this site in different environments, we have modeled the *spoke*-isomers of the dirhodium unit with planar polyaromatic ligands, $C_{10}H_8$ and $C_{12}H_8$ (Figure 3). They will be later compared with the *spoke*-complexes of the $C_{20}H_{10}$-bowl and the C_{60}-ball.

Although such adducts have not been observed experimentally, both $[Rh_2(O_2CCF_3)_4\cdot(\eta^2\text{-}spoke\text{-}C_{10}H_8)]$ (**4b**) and $[Rh_2(O_2CCF_3)_4\cdot(\eta^2\text{-}spoke\text{-}C_{12}H_8)]$ (**5c**) were found to be true minima on the PES. Their bonding energies of 9.76 and 13.08 kcal/mol for **4b** and **5c**, respectively, indicate that the *spoke*-bond in planar polyarenes could be involved in metal binding. However, the *spoke*-isomers are less stable than the corresponding *rim*-adducts of the same polyarene (Table 2). The low values of bonding energy are consistent with very small elongations of the Rh−Rh bond length and the coordinated C−C bond of a polyaromatic molecule (Δ is 0.015 Å in **5c** and 0.007 Å in **4b**). The long Rh−C bond distances in **4b** and **5c** (Table 2) are also

SCHEME 3: Schematic Representations of the Interacting MOs in (a) [$Rh_2(O_2CCF_3)_4\cdot(\eta^2$-$C_6H_6)$] (3), (b) [$Rh_2(O_2CCF_3)_4\cdot(\eta^2$-*rim*-$C_{10}H_8)$] (4a), (c) [$Rh_2(O_2CCF_3)_4\cdot(\eta^2$-*rim*-$C_{12}H_8)$] (5a), (d) [$Rh_2(O_2CCF_3)_4\cdot(\eta^2$-*hub*-$C_{12}H_8)$] (5b), (e) [$Rh_2(O_2CCF_3)_4\cdot(\eta^2$-*spoke*-$C_{10}H_8)$] (4b), and (*f*) [$Rh_2(O_2CCF_3)_4\cdot(\eta^2$-*spoke*-$C_{12}H_8)$] (5c)

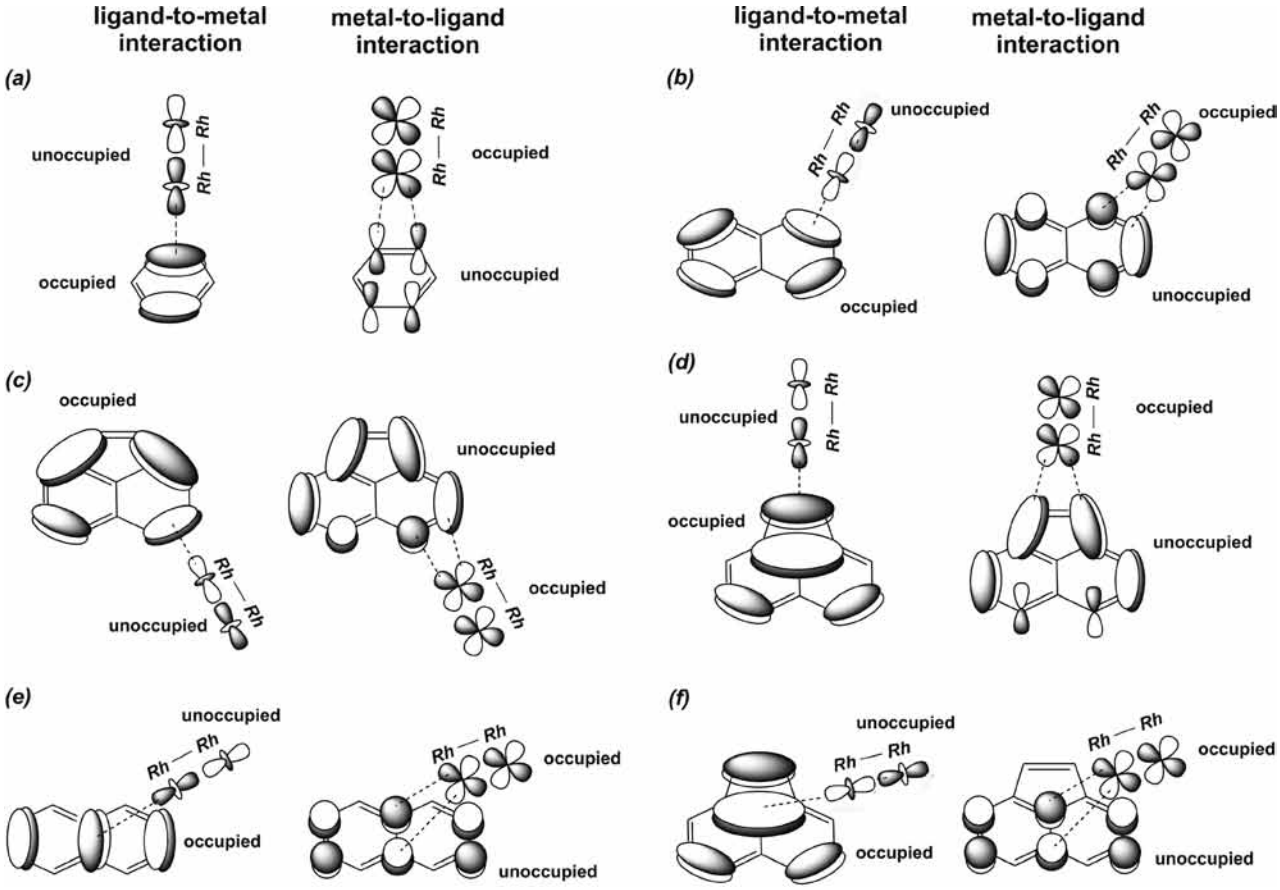

in agreement with the low stability of the *spoke*-isomers. In **5c**, there is a strong inequivalence of the two Rh—C bond length distances (Δ is 0.341 Å vs 0.092 in **4b**). The asymmetry in metal—carbon interactions has previously been seen in the unique diruthenium *hub*-corannulene complex isolated experimentally,[44] where hapticity of metal—π—arene interaction was finally assigned to η^1.

An in-depth investigation of the nature of the interaction between the dirhodium core and a polyarene in the *spoke*-adducts in terms of the NBO method showed that both M → L and L → M interactions in **4b** are very low (4.29 and 2.71 kcal/mol). In the case of **5c**, the M → L contribution is also small (4.54 kcal/mol), whereas the L → M donation of 16.03 kcal/mol is higher than in the benzene adduct **3** (13.65 kcal/mol). The latter shows the lowest stability in this series but was nevertheless isolated and structurally characterized.[40a] Thus, the addition of a fused five-membered ring to a naphthalene core results in the noticeable increase of a donating ability of the *spoke* carbon—carbon site in acenaphthylene.

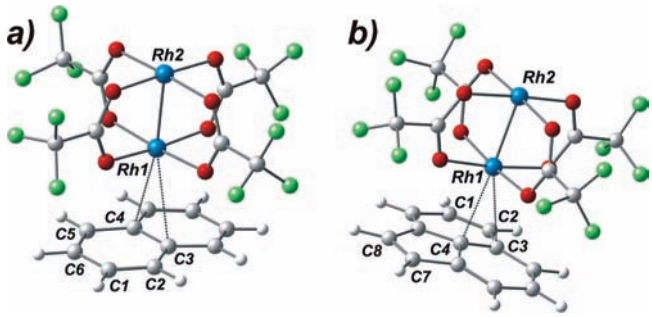

Figure 3. Equilibrium geometry configurations of (a) [$Rh_2(O_2CCF_3)_4\cdot(\eta^2$-*spoke*-$C_{10}H_8)$] (**4b**) and (b) [$Rh_2(O_2CCF_3)_4\cdot(\eta^2$-*spoke*-$C_{12}H_8)$] (**5c**), along with the corresponding labeling schemes.

A detailed analysis of the electronic structures of **4b** and **5c** has demonstrated the similarity and differences in bonding of these adducts (see Supporting Information, Figures S39 and S41 for their MO interaction diagrams). In **4b**, the L → M interaction is formed by HOMO - 1 of naphthalene and LUMO (σ* MO mainly localized at the dimetal core) of [$Rh_2(O_2CCF_3)_4$]. In **5c**, the L → M contribution is provided by HOMO of acenaphthylene and LUMO of the dirhodium unit. Interestingly, HOMO - 1 of naphthalene is equally distributed over the *spoke* carbon—carbon bond providing a symmetrical η^2-coordination mode in the corresponding dirhodium adduct. At the same time, HOMO of acenaphthylene involves one *hub*-carbon atom without contribution from the other carbon atom of the *spoke* bond. The L → M bonding should therefore be described as the interaction of the Rh_2^{4+} core with the *hub*-carbon atom of acenaphthylene only (Scheme 3f). However, the M → L contributions in **4b** and **5c** are the 4 electrons—3 orbitals interactions involving both carbon atoms of the *spoke* site.

Adducts with π-Bowls, $C_{20}H_{10}$ and $C_{30}H_{12}$. From planar polyaromatic systems, we have moved to open geodesic polyarenes[45] having curved unsaturated carbon surfaces, namely, corannulene and the C_3-symmetric hemifullerene (Scheme 2). Although corannulene is quite shallow and maps only ca. 30 % of the C_{60}-surface, the hemifullerene has a greater curvature and represents a symmetrical half of the fullerene. The estimated

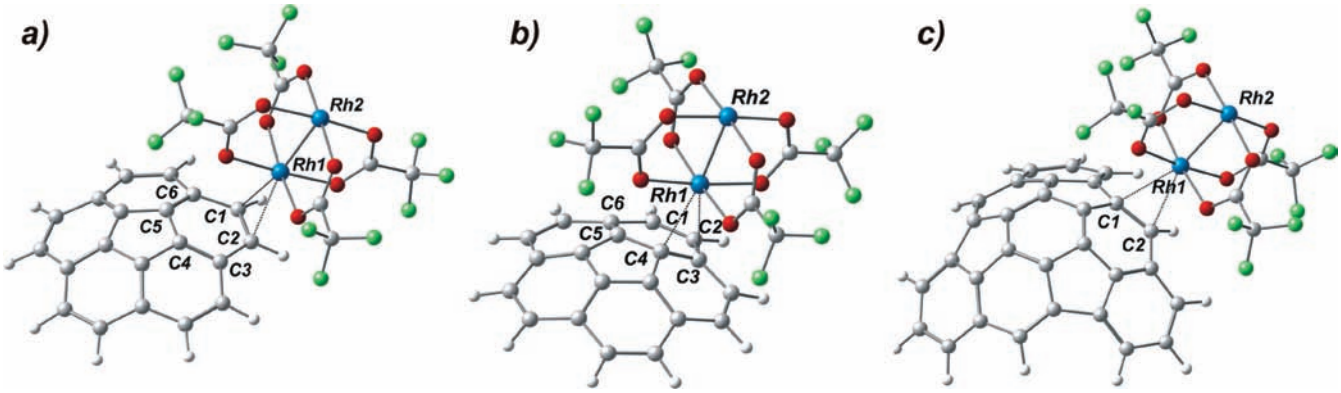

Figure 4. Equilibrium geometry configurations of (a) $[Rh_2(O_2CCF_3)_4\cdot(\eta^2\text{-}rim\text{-}exo\text{-}C_{20}H_{10})]$ (**7a**), (b) $[Rh_2(O_2CCF_3)_4\cdot(\eta^2\text{-}spoke\text{-}exo\text{-}C_{20}H_{10})]$ (**7b**), and (c) $[Rh_2(O_2CCF_3)_4\cdot(\eta^2\text{-}rim\text{-}exo\text{-}C_{30}H_{12})]$ (**8**), along with the corresponding labeling schemes.

TABLE 3: Selected Calculated Parameters for $C_{20}H_{10}$, $C_{30}H_{12}$, C_{60}, and Their Adducts with $[Rh_2(O_2CCF_3)_4]$, 7−9

	compound						
parameter	$C_{20}H_{10}$	$C_{30}H_{12}$	C_{60}	**7a**	**7b**	**8**	**9**
Rh(1)—Rh(2)				2.425	2.421	2.430	2.424
Rh(1)—C(1a)[a]				2.473	2.850	2.470	2.436
Rh(1)—C(2b)[a]				2.491	2.450	2.562	2.432
C(1)—C(2)	1.385	1.378	1.391	1.410	1.385	1.410	1.409
C(3)—C(4)	1.382				1.400		
order, Rh(1)—Rh(2)				0.637	0.653	0.634	0.657
order, C(1)—C(2)	1.627	1.529	1.384	1.485	1.617	1.416	1.302
order, C(3)—C(4)					1.260		
charge, Rh(1)				+0.929	+0.938	+0.926	+0.879
charge, Rh(2)				+0.881	+0.891	+0.883	+0.863
charge, C(1)	−0.180	−0.059	−0.00	−0.212	−0.133	−0.036	−0.038
charge, C(2)	−0.180	−0.147	−0.00	−0.206	−0.190	−0.036	−0.037
charge, C(3)	−0.049				−0.013		
charge, C(4)	−0.014				−0.128		
$E^{(2)}$(M→L), kcal/mol				10.53	8.49	9.95	16.88
$E^{(2)}$(L→M), kcal/mol				40.79	28.16	37.79	40.95
E(bonding), kcal/mol				18.79	16.56	18.34	50.13

[a] These carbon atoms are directly bound to a rhodium center. In *rim*-isomers, they are designated as C(1) and C(2), and in *spoke*-isomers as C(3) and C(4).

bowl depth of $C_{20}H_{10}$ is 0.875 Å versus 2.43 Å for $C_{30}H_{12}$.[11] Crystalline complexes of $[Rh_2(O_2CCF_3)_4]$ with both bowls have been isolated and structurally characterized in our group,[11] but no theoretical description of bonding was provided at that time. They were found to exhibit extended 1D and 2D (corannulene) and 3D (hemifullerene) structures built on the bridging μ_2-η^2:η^2, μ_3-η^2:η^2:η^2, and μ_4-η^2:η^2:η^2:η^1 modes of bowls, respectively. The experimental X-ray diffraction data clearly indicated that the electrophilic rhodium(II) centers bind only the outer rim C—C bonds of these bowl-shaped polyarenes. It should be mentioned that Ag^+ ions also coordinate corannulene via rim bonds in an η^2-fashion.[46] Several crystallographically characterized η^6-corannulene complexes of Ir(I), Rh(I),[47] Ru(I), and Ir(II)[48] can be mentioned here, but those are beyond the scope of this discussion. Herein, we have tested computationally the reactivity of the *rim*-sites of $C_{20}H_{10}$ and $C_{30}H_{12}$ as well as those of the *spoke*-bond in corannulene toward the η^2-coordination of highly electrophilic $[Rh_2(O_2CCF_3)_4]$.

Because there are two distinct faces in bowl-shaped polyarenes (*convex* or *exo* and *concave* or *endo*), two possible ways of metal coordination should be differentiated. The extended structures revealed by X-ray crystallography for the rhodium(II) complexes of $C_{20}H_{10}$ and $C_{30}H_{12}$ did not allow us to identify the preference of *convex* versus *concave* surfaces of these bowls for metal binding.[49] However, the recently isolated discrete ruthenium(I) complexes of corannulene[44,50] along with other reported examples, all exhibited *exo* coordination of a metal to $C_{20}H_{10}$ and thus showed the general preference of the *convex* (*exo*) face of the corannulene bowl for metal binding.[51] Therefore, the *exo*-isomers of $[Rh_2(O_2CCF_3)_4]$-adducts with $C_{20}H_{10}$ and $C_{30}H_{12}$ have been computed and analyzed in this work.

The good agreement found between the calculated and experimental geometrical parameters[11] of $[Rh_2(O_2CCF_3)_4\cdot(\eta^2\text{-}rim\text{-}exo\text{-}C_{20}H_{10})]$ (**7a**) and $[Rh_2(O_2CCF_3)_4\cdot(\eta^2\text{-}rim\text{-}exo\text{-}C_{30}H_{12})]$ (**8**) (Figure 4, Supporting Information, Tables S20 and S22) demonstrates that the PBE0 functional is suitable for accurate description of complexes formed by bowl-shaped polyaromatic hydrocarbons with polynuclear transition metal units. Despite the fact that the geometries of discrete complexes are compared with extended crystal structures, the maximum differences between the calculated and experimental parameters for **7a** (0.027 and 0.065 Å for 1D and 2D, respectively) and **8** (0.047 Å) are reasonable.

The geometric and electronic structures of **7a** and **8** are close (Table 3). The specific feature found in adducts with planar arenes, namely, the 4 electrons−3 orbitals M → L interaction, also describes bonding in **7a** and **8** (Supporting Information, Figures S43 and S46). In both adducts, coordination results in an elongation of the Rh—Rh bond lengths because of the L →

M electron donation and, as a consequence, an increase of occupancy of σ^* antibonding MO centered at the dirhodium core.

As mentioned above, the site provided by a polyarene for metal binding is determined by the topology of frontier molecular orbitals of a ligand and the localization of its highest π-bond order. In **7a** and **8**, both methods predict the *rim* of a bowl as the preferential coordination site (Supporting Information, Table S28 and Figures S30 and S31). However, although in corannulene, all *rim* carbon−carbon bonds are equivalent, the metal coordination to a $C_{30}H_{12}$-bowl is site specific (Figure 4c).

Bonding energies are very close for the η^2-*rim* adducts of corannulene (18.79 kcal/mol, **7a**) and hemifullerene (18.34 kcal/mol, **8**) but slightly lower than those for the pyrene and acenaphthylene complexes (Tables 2 and 3). Hence, a significant increase in curvature of a π-bowl when going from $C_{20}H_{10}$ to $C_{30}H_{12}$ showed no effect on the *rim*-adducts of $[Rh_2(O_2CCF_3)_4]$, whereas some decrease in stability of **7a** and **8** is observed in comparison with the analogues based on planar polyarenes.

So far, there are no experimental examples of *spoke* coordination for the Rh_2^{4+} core; therefore, it was informative to computationally test the potential reactivity of this internal site of a corannulene bowl and to compare the results with planar polyarenes and the C_{60}-fullerene. Similarly to the *spoke*-adducts of naphthalene and acenaphthylene, $[Rh_2(O_2CCF_3)_4\cdot(\eta^2\text{-}spoke\text{-}exo\text{-}C_{20}H_{10})]$ has been found to be a true minimum on the PES. Moreover, its bonding energy (16.56 kcal/mol, **7b**) is only slightly lower than that of the corresponding *rim*-isomer (18.79 kcal/mol, **7a**). The stability of the *spoke*-adduct of corannulene is higher compared to that of the corresponding analogues with planar polyarenes (9.76 kcal/mol for the naphthalene adduct, **4b**, and 13.08 kcal/mol for the acenaphthylene complex, **5c**). Similarly to **5c**, a significant inequivalence of the two Rh−C bond length distances (Δ is 0.40 Å) is found in **7b**. As mentioned above, the asymmetric coordination has previously been seen in the $[Ru_2(O_2C(3,5\text{-}CF_3)_2C_6H_3)_2(CO)_5\cdot(\eta^1\text{-}hub\text{-}exo\text{-}C_{20}H_{10})]$ complex.[44] However, the main difference between that *hub*-adduct of $C_{20}H_{10}$ and **7b** is the nature of their metal−π interactions. The MO diagram of $[Rh_2(O_2CCF_3)_4\cdot(\eta^2\text{-}spoke\text{-}exo\text{-}C_{20}H_{10})]$ (Supporting Information, Figure S44) shows the presence of the 4 electrons−3 orbitals for the M → L interaction that involves both *spoke* carbon atoms of corannulene. In contrast, only the *hub*-carbon atom of $C_{20}H_{10}$ was found to be engaged in bonding in the diruthenium complex.

The M → L contributions are low in both **5c** and **7b** (4.54 and 8.49 kcal/mol, respectively), but the higher bonding energy in **7b** is mainly provided by a greater L → M donation (16.03 vs 28.16 kcal/mol). Thus, the donor−acceptor ability of the internal *spoke*-site of a bowl-shaped corannulene is noticeably greater compared to the planar polyaromatic systems, with this effect being even more pronounced in the closed C_{60}-fullerene, as shown below.

Adduct with the C_{60}-fullerene. The logical step completing the series of rhodium adducts with planar polyarenes and π-bowls mapping onto the C_{60}-surface is to consider the fullerene itself. The latter is well known to have two types of carbon−carbon bonds at the junction between two six-membered rings (6:6) and between six- and five-membered rings (5:6). All experimental structural data show the metal binding to the (6:6) sites exclusively.[43,52] This is consistent with the topology of frontier molecular orbitals of C_{60}, because its five highest occupied degenerate MOs (HOMOs) as well as three lowest unoccupied MOs (LUMOs) are localized at the (6:6) sites

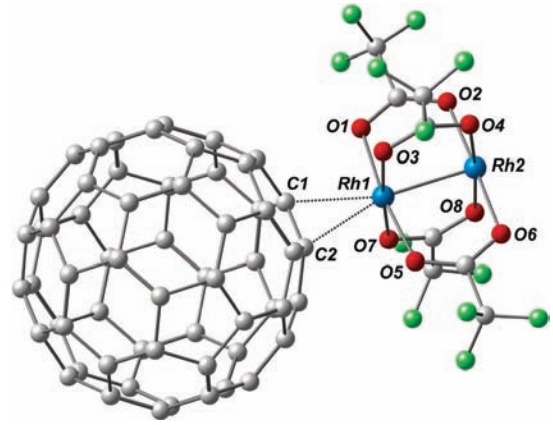

Figure 5. Equilibrium geometry configuration of $[Rh_2(O_2CCF_3)_4\cdot(\eta^2\text{-}C_{60})]$ (**9**), along with the corresponding labeling scheme.

(Supporting Information, Figure S32). Hence, we modeled only one adduct with the rhodium(II) center coordinated to the (6:6) bond at the C_{60}-surface, namely, $[Rh_2(O_2CCF_3)_4\cdot(\eta^2\text{-}C_{60})]$ (**9**, Figure 5).

The X-ray crystallographic data for $[Rh_2(O_2CCF_3)_4\cdot(\eta^2\text{-}C_{60})]$ are not available; however, all theoretical results presented above clearly indicate good applicability of the selected DFT level for modeling these systems. A comparison of geometrical parameters of **9** with those of the individual molecules, C_{60} and $[Rh_2(O_2CCF_3)_4]$ (Table 3), shows that coordination leads to a noticeable elongation of the Rh−Rh bond distance in **9** (2.424 vs 2.385 Å in the unligated $[Rh_2(O_2CCF_3)_4]$ dimer). Similarly to other cases, the adduct formation results in the elongation of the coordinated C(1)−C(2) bond of the C_{60}-ligand from 1.391 to 1.409 Å. The two Rh−C bond lengths in **9** are close, 2.436 and 2.432 Å, indicating a symmetrical η^2-coordination of the C_{60}-fullerene by the dirhodium unit. In contrast, the isoelectronic Ru_2^{2+} unit was found to coordinate to C_{60} in an asymmetric mode.[53] Consistent with the highest stability of the fullerene-based complex, the Rh−C bond length distances in **9** are the shortest in the whole series considered here, except for the *hub*-acenaphthylene adduct **5b**. Specifically, the bonding energy of 50.13 kcal/mol in $[Rh_2(O_2CCF_3)_4\cdot(\eta^2\text{-}C_{60})]$ is more than twice greater than the estimated values for all other dirhodium adducts (Tables 1−3). For comparison, the bonding energy of the *spoke*-adduct of corannulene, in which rhodium(II) is bound to the same junction of the two six-membered rings, is only 16.56 kcal/mol. A significant difference in bonding energy between the C_{60}-ball and the $C_{20}H_{10}$-bowl has also been seen in the corresponding diruthenium(I) adducts.[53] The detailed NBO analysis of the electronic structure of $[Rh_2(O_2CCF_3)_4\cdot(\eta^2\text{-}C_{60})]$ allowed us to rationalize its high bonding energy. The L → M contribution of 40.95 kcal/mol is one of the largest in **9**, with the M → L interaction energy of 16.88 kcal/mol also being noticeably greater compared to other adducts (Tables 1−3 and Supporting Information, Table S32). It can also be mentioned here that the energy gap between the interacting orbitals is smaller in the fullerene adduct, because LUMOs of C_{60} (−0.1771 au) lie significantly lower than those of other π-ligands discussed in this work. This results in the stronger M → L interaction in $[Rh_2(O_2CCF_3)_4\cdot(\eta^2\text{-}C_{60})]$ compared to other adducts.

Thus, the C_{60}-fullerene exhibits greater acceptor and donor abilities than open geodesic polyarenes ($C_{20}H_{10}$, $C_{30}H_{12}$), planar aromatic systems (C_6H_6, $C_{10}H_8$, $C_{12}H_8$, $C_{16}H_{10}$), and linear hydrocarbons with isolated multiple carbon−carbon bonds (C_2H_2, C_2H_4). Moreover, a comparison of charge distribution

in the C_{60}-adduct with that of parent molecules showed slight polarization of the axially bound fullerene. The originally neutral carbon atoms of C_{60} become negatively charged in **9** (−0.037 and −0.038 for C(1) and C(2), respectively). This can be explained by (i) polarization of a coordinated ligand induced by positively charged metal center and (ii) electron transfer from the occupied MOs centered at the Rh_2^{4+} core to the unoccupied MOs of C_{60}. As it stems from the NBO analysis of **9**, the L → M contribution is significantly greater than the M → L one. Thus, the induced polarization of the coordinated C_{60}-fullerene seems to play the major role. This is also confirmed by a quick look at the charges of other carbon atoms of C_{60}, which became slightly positive in **9** (Supporting Information, Tables S24 and S27).

General Trends and Concluding Remarks

Because this is the first systematic theoretical investigation of rhodium(II)−π complexation with a number of unsaturated hydrocarbons having variable geometries, sizes, electronic structures, aromatic conjugation, and curvatures, it is informative to make some general comparisons for the whole series. An analysis of all MO interaction diagrams (see Supporting Information) shows that the nature of the interactions between the electrophilic Rh_2^{4+} unit and all studied π-systems is very similar. However, the resulting products show different stability with bonding energies ranging broadly from 14.59 (for the least stable benzene adduct) to 50.13 kcal/mol (for the most stable fullerene complex). The stability of the acetylene adduct is also low (16.60 kcal/mol), but a replacement of acetylene by ethylene leads to an increase in bonding energy to 20.59 kcal/mol. Polyaromatic hydrocarbons form more stable η^2-adducts with $[Rh_2(O_2CCF_3)_4]$ than benzene and acetylene, with their bonding energies being close to that of the ethylene complex. Interestingly, imposing curvature to polyaromatic surfaces in corannulene and hemifullerene leads to a slight decrease in stability of their η^2-*rim*-complexes, as compared to planar acenaphthylene and pyrene.

Generally, an increase in adduct stability is accompanied by a decrease of metal−metal bond orders (or elongation of the Rh−Rh bond length) because of the donation of electrons from HOMO of ligands to σ^* antibonding MO centered at the dirhodium core. Thus, the least stable adducts with acetylene and benzene are characterized by the shortest bond distance between the two rhodium(II) centers. Correspondingly, the coordinated carbon−carbon bond length in axially bound ligands shows the greatest elongation in the most stable adducts. At the same time, no evident correlation between the overall stability and the calculated or experimental Rh−C bond length was found.

Interesting trends have been revealed when separate M → L and L → M contributions to bonding were considered. In general, the most stable adducts show the highest ligand-to-metal interaction energy. Thus, in terms of their donating abilities toward the Rh_2^{4+} core, the selected ligands follow the order: *hub*-$C_{12}H_8$ (51.54) > C_{60} (40.95) ≈ *rim*-$C_{20}H_{10}$ (40.79) > *rim*-$C_{10}H_8$ (39.59) > $C_{16}H_{10}$ (38.41) ≈ *rim*-$C_{12}H_8$ (38.11) ≈ C_2H_4 (37.91) ≈ $C_{30}H_{12}$ (37.79) > C_2H_2 (24.10) > C_6H_6 (13.65). In contrast, the energies of M → L back donations vary in a smaller range of 6.46−16.88 kcal/mol. Considering the accepting abilities of the same set of ligands, they follow the order: C_{60} (16.88) > C_6H_6 (12.34) > C_2H_4 (10.94) > *rim*-$C_{20}H_{10}$ (10.53) ≈ *hub*-$C_{12}H_8$ (10.35) > $C_{30}H_{10}$ (9.95) > $C_{16}H_{10}$ (7.97) > C_2H_2 (7.50) ≈ *rim*-$C_{10}H_8$ (7.42) > *rim*-$C_{12}H_8$ (6.46). The C_{60}-fullerene acts as the best donor and acceptor in this series.

Importantly, these trends depend on the ligand coordination site and the nature of metal. The latter can be clearly illustrated by a direct comparison of Rh(II) and Ru(I) binding to the *rim* site of corannulene. The calculated energies of the L → M contributions for the significantly softer ruthenium(I) complexes are much lower than for very Lewis acidic rhodium(II). For example, these values for $[Ru_2(O_2CCF_3)_2(CO)_4\cdot(\eta^2\text{-}rim\text{-}exo\text{-}C_{20}H_{10})]$ and $[Ru_2(O_2C(3,5\text{-}CF_3)_2C_6H_3)_2(CO)_5\cdot(\eta^2\text{-}rim\text{-}exo\text{-}C_{20}H_{10})]$ are 21.77[50] and 25.22 kcal/mol,[44] respectively, compared to 40.79 kcal/mol for $[Rh_2(O_2CCF_3)_4\cdot(\eta^2\text{-}rim\text{-}exo\text{-}C_{20}H_{10})]$. At the same time, the energies of the M → L back donation are greater in the above ruthenium complexes, being 14.37 and 16.90 kcal/mol (vs 10.53 kcal/mol in the rhodium(II) adduct). Very similar trends are observed for the diruthenium(I)[53] and dirhodium(II)-based fullerene complexes. Again, the L → M interaction energy is lower in the ruthenium(I) adduct (24.29 vs 40.95 kcal/mol in the rhodium(II) complex), whereas the M → L contribution is significantly higher in the former (32.52 vs 16.88 kcal/mol in $[Rh_2(O_2CCF_3)_4\cdot(\eta^2\text{-}C_{60})]$).

Regarding the specific ligand coordination site, two Ru(I) complexes can be compared, namely, $[Ru_2(O_2C(3,5\text{-}CF_3)_2C_6H_3)_2(CO)_5\cdot(\eta^2\text{-}rim\text{-}exo\text{-}C_{20}H_{10})]$ and $[Ru_2(O_2C(3,5\text{-}CF_3)_2C_6H_3)_2(CO)_5\cdot(\eta^1\text{-}hub\text{-}exo\text{-}C_{20}H_{10})]$.[44] For the latter, the energy contributions of L → M (19.13 kcal/mol) and M → L (8.59 kcal/mol) are lower than those for the *rim*-bound corannulene complex (25.22 and 16.90 kcal/mol, respectively). This is in agreement with the experimentally observed *rim*-preference of $C_{20}H_{10}$ for coordination of electrophilic metal centers.

For the highly Lewis acidic Rh_2^{4+} core, no complexation to the internal s*poke* site has yet been seen experimentally, but computational evaluation of its reactivity allows us to make a general comparison for planar and nonplanar polyaromatic surfaces. For naphthalene, acenaphthylene, and corannulene, the calculated data unambiguously indicate the preference of a *rim*-bond over a *spoke*-site for coordination of $[Rh_2(O_2CCF_3)_4]$. This is supported by a difference in bonding energies of the corresponding *rim* and *spoke* isomers that is greater for planar polyarenes (8.1 and 4.7 kcal/mol for naphthalene and acenaphthylene, respectively) compared to only 2.2 kcal/mol for corannulene. The latter result illustrates relative stability of the *spoke*-corannulene isomer and implies that such π-complexes are feasible. Interestingly, only in the *spoke*-adduct with naphthalene (**4b**) the symmetrical η^2-coordination of a π-ligand has been found. In contrast, the *spoke*-adducts of $C_{12}H_8$ (**5c**) and $C_{20}H_{10}$ (**7b**) show an asymmetry in coordination, which is rationalized when a detailed description of bonding is provided. Although the M → L donation in **5c** and **7b** involves both carbon atoms of a *spoke* bond, the inequivalence in Rh−C binding is dictated by the L → M contributions that include only the *hub*-carbon atom of a polyarene. For the given series of adducts, the L → M contributions are found to play a major role. Thus, the revealed differences in stability of *rim* and *spoke* pairs are arising from a significantly greater L → M interaction energy found in all *rim*-bound isomers (Tables 2 and 3).

It is worth mentioning that coordination of π-ligands, both conjugated aromatic or molecules with isolated multiple C−C bonds, results in perturbation of charge distribution in the dimetal core in comparison with parent $[Rh_2(O_2CCF_3)_4]$. Specifically, the charge at the rhodium center involved in coordination becomes more positive than that at the open metal end. Only in the fullerene complex, despite the strongest M → L interaction, this difference is rather small ($\Delta = 0.016$). In other monoadducts, a disparity in charges of the two rhodium centers is observed. This can be clearly illustrated by comparing a very

stable acenaphthylene adduct, $[Rh_2(O_2CCF_3)_4 \cdot (\eta^2\text{-}hub\text{-}C_{12}H_8)]$, having charges of +0.927 and +0.855 ($\Delta = 0.072$), with the least stable benzene analogue, $[Rh_2(O_2CCF_3)_4 \cdot (\eta^2\text{-}C_6H_6)]$, for which Δ is 0.045. Therefore, the overall interaction between the Rh_2^{4+} unit and the selected π-ligands consists of two major components: (i) Coulomb interaction between the positively charged rhodium center and an induced dipole moment of axially bound hydrocarbons and (ii) donor−acceptor interactions between the dimetal core and π-type MOs of ligands with a strong orbital control (having both L → M and M → L contributions with the former being a major contributor to the bonding). It is noteworthy that an increase in hardness of the dimetal core when moving from Ru_2^{2+} to Rh_2^{4+} leads to a decrease of donor−acceptor contributions accompanied by an increase of Coulomb forces.

Acknowledgment. The support of this work by the Donors of the American Chemical Society Petroleum Research Fund (PRF 42910-AC3) and the National Science Foundation Career Award (CHE-0546945) is gratefully acknowledged. The authors also thank Anne Shelton and Eric Warnke at the University at Albany's Research IT group for their support in parallel large-scale cluster calculations and Dr. Anastasia V. Bochenkova at Moscow State University for helpful advice and kind assistance in solution of the convergence problem for large size systems. The access to computational power of the Beowulf cluster provided by Prof. Peter Burger (Institute of Inorganic and Applied Chemistry, University of Hamburg) is also acknowledged.

Supporting Information Available: Computation details, MO interaction diagrams for all adducts, MO diagrams, and tabular materials. This material is available free of charge via the Internet at http://pubs.acs.org.

References and Notes

(1) (a) Calderazzo, F.; Pampaloni, G. *J. Organomet. Chem.* **1995**, *500*, 47. (b) Ma, J. C.; Dougherty, D. A. *Chem. Rev.* **1997**, *97*, 1303. (c) Kim, K. S.; Tarakeshwar, P.; Lee, J. Y. *Chem. Rev.* **2000**, *100*, 4145. (d) Gokel, G. W.; Barbour, L. J.; De Wall, S. L.; Meadows, E. S. *Coord. Chem. Rev.* **2001**, *222*, 127. (e) Zaric, S. D. *Eur. J. Inorg. Chem.* **2003**, 2197.

(2) (a) Fernandez, D.; Ghanta, A.; Kauffman, G. W.; Sanguinetti, M. C. *J. Biol. Chem.* **2004**, *279*, 10120. (b) Wintjens, R.; Noel, C.; May, A. C. W.; Gerbod, D.; Dufernez, F.; Capron, M.; Viscogliosi, E.; Rooman, M. *J. Biol. Chem.* **2004**, *279*, 9248. (c) Cashin, A. L.; Petersson, E. J.; Lester, H. A.; Dougherty, D. A. *J. Am. Chem. Soc.* **2005**, *127*, 350.

(3) (a) Woodgate, P. D. *Adv. Detailed Reac. Mech.* **1995**, *4*, 93. (b) Kuendig, E. P.; Pape, A. *Top. Organomet. Chem.* **2004**, *7*, 71.

(4) Ritleng, V.; Sirlin, C.; Pfeffer, M. *Chem. Rev.* **2002**, *102*, 1731.

(5) Rigby, J. H.; Kondratenko, M. A. *Top. Organomet. Chem.* **2004**, *7*, 181.

(6) Some recent works:(a) Gapeev, A.; Dunbar, R. C. *J. Phys. Chem. A* **2000**, *104*, 4084. (b) Ruan, C.; Rodgers, M. T. *J. Am. Chem. Soc.* **2004**, *126*, 14600. (c) Zhu, W.; Luo, X.; Puah, C. M.; Tan, X.; Shen, J.; Gu, J.; Chen, K.; Jiang, H. J. *J. Phys. Chem. A* **2004**, *108*, 4008. (d) Siu, F. M.; Ma, N. L.; Tsang, C. W. *Chem.—Eur. J.* **2004**, *10*, 1966. (e) Ruan, C.; Yang, Z.; Hallowita, N.; Rodgers, M. T. *J. Phys. Chem. A* **2005**, *109*, 11539. (f) Vijay, D.; Sastry, G. N. *Phys. Chem. Chem. Phys.* **2008**, *10*, 582.

(7) (a) Deubel, D. V. *Organometallics* **2002**, *21*, 4303. (b) Dunbar, R. C. *J. Phys. Chem. A* **2002**, *106*, 7328. (c) Gapeev, A.; Dunbar, R. C. *J. Am. Soc. Mass Spectrom.* **2002**, *13*, 477. (d) Jaeger, T. D.; van Heijnsbergen, D.; Klippenstein, S. J.; von Helden, G.; Meijer, G.; Duncan, M. A. *J. Am. Chem. Soc.* **2004**, *126*, 10981. (e) Jaeger, T. D.; Pillai, E. D.; Duncan, M. A. *J. Phys. Chem. A* **2004**, *108*, 6605. (f) Zhang, S.-L.; Liu, L.; Fu, Y.; Guo, Q.-X. *J. Mol. Struct.* **2005**, *757*, 37.

(8) (a) Nunzi, F.; Sgamellotti, A.; Re, N. *Organometallics* **2002**, *21*, 2219. (b) Kameno, Y.; Ikeda, A.; Nakao, Y.; Sato, H.; Sakaki, S. *J. Phys. Chem. A* **2005**, *109*, 8055. (c) Sastry, G. N. *J. Mol. Str.: Theochem* **2006**, *771*, 141. (d) Gal'pern, E. G.; Stankevich, I. V. *Russ. J. Phys. Chem. A* **2008**, *82*, 982.

(9) (a) Petrie, S.; Stranger, R. *Inorg. Chem.* **2004**, *43*, 2597. (b) Zhang, S.-L.; Liu, L.; Fu, Y.; Guo, Q.-X. *J. Mol. Str.: Theochem* **2005**, *757*, 37. (c) Deubel, D. V. *J. Am. Chem. Soc.* **2006**, *128*, 1654. (d) Laberquerie, P.; Benard, M.; Rohmer, M.-M. *Inorg. Chem.* **2007**, *46*, 5283. (e) Vega, A.; Saillard, J.-Y. *Inorg. Chem.* **2007**, *46*, 3295.

(10) (a) Cotton, F. A.; Dikarev, E. V.; Petrukhina, M. A. *Angew. Chem., Int. Ed.* **2000**, *39*, 2362. (b) Cotton, F. A.; Dikarev, E. V.; Petrukhina, M. A. *Angew. Chem., Int. Ed.* **2001**, *40*, 1521.

(11) (a) Petrukhina, M. A.; Andreini, K. W.; Mack, J.; Scott, L. T. *Angew. Chem., Int. Ed.* **2003**, *42*, 3375. (b) Petrukhina, M. A.; Andreini, K. W.; Peng, L.; Scott, L. T. *Angew. Chem., Int. Ed.* **2004**, *43*, 5477.

(12) (a) Dikarev, E. V.; Andreini, K. W.; Petrukhina, M. A. *Inorg. Chem.* **2004**, *43*, 3219. (b) Petrukhina, M. A.; Filatov, A. S.; Sevryugina, Y.; Andreini, K. W.; Takamizawa, S. *Organometallics* **2006**, *25*, 2135. (c) Filatov, A. S.; Petrukhina, M. A. *J. Organomet. Chem.* **2008**, *693*, 1590.

(13) Chifotides, H. T.; Dunbar, K. R. Rhodium Compounds. *Multiple Bonds Between Metal Atoms*, 3rd Ed.; Cotton, F. A., Murillo, C. A., Walton, R. A. , Eds.; Springer Sci. Inc.: New York, 2005; pp 465−589.

(14) (a) Doyle, M. P.; Forbes, D. C. *Chem. Rev.* **1998**, *98*, 911. (b) Doyle, M. P.; Ren, T. *Prog. Inorg. Chem.* **2001**, *49*, 113. (c) Timmons, D. J.; Doyle, M. P. Chiral Dirhodium(II) Catalysts and Their Applications. *Multiple Bonds Between Metal Atoms* 3rd Ed.; Cotton, F. A., Murillo, C. A., Walton, R. A., Eds.; Springer Sci. Inc.: New York, 2005; pp 591−632. (d) Davies, H. M. L. *Angew. Chem., Int. Ed.* **2006**, *45*, 6422. (e) Davies, H. M. L.; Hedley, S. J. *Chem. Soc. Rev.* **2007**, *36*, 1109. (f) Hansen, J.; Davies, H. M. L. *Coord. Chem. Rev.* **2008**, *252*, 545.

(15) (a) Chifotides, H. T.; Dunbar, K. R. *Acc. Chem. Res.* **2005**, *38*, 146. (b) Chifotides, H. T.; Dunbar, K. R. *J. Am. Chem. Soc.* **2007**, *129*, 12480. (c) Chifotides, H. T.; Dunbar, K. R. *Chem.—Eur. J.* **2008**, *14*, 9902.

(16) (a) Bradley, P. M.; Fu, P. K.-L.; Turro, C. *Comments Inorg. Chem.* **2001**, *22*, 393. (b) Angelez-Boza, A. M.; Bradley, P. M.; Fu, P. K.-L.; Shatruk, M.; Hilfiger, M. G.; Dunbar, K. R.; Turro, C. *Inorg. Chem.* **2005**, *44*, 7262. (c) Lutterman, D. A.; Fu, P. K.-L.; Turro, C. *J. Am. Chem. Soc.* **2006**, *12*, 8–738. (d) Aguirre, J. D.; Lutterman, D. A.; Angelez-Boza, A. M.; Dunbar, K. R.; Turro, C. *Inorg. Chem.* **2007**, *46*, 7494.

(17) (a) Sigal, I. S.; Mann, K. R.; Gray, H. B. *J. Am. Chem. Soc.* **1980**, *102*, 7252. (b) Heyduk, A. F.; Nocera, D. G. *Science* **2001**, *293*, 1939.

(18) (a) Cotton, F. A.; Lin, C.; Murillo, C. A. *Acc. Chem. Res.* **2001**, *34*, 759. (b) Holliday, B. J.; Mirkin, C. A. *Angew. Chem., Int. Ed.* **2001**, *40*, 2022. (c) Cotton, F. A.; Lin, C.; Murillo, C. A. *Proc. Nat. Acad. Sci. U.S.A.* **2002**, *99*, 4810. (d) Chisholm, M. H. *Proc. Nat. Acad. Sci. U.S.A.* **2007**, *104*, 2563.

(19) Deubel, D. V.; Chifotides, H. T. *Chem. Commun.* **2007**, 3438.

(20) Petrukhina, M. A. *Coord. Chem. Rev.* **2007**, *251*, 1690.

(21) (a) Perdew, J. P.; Burke, K.; Ernzerhof, M. *Phys. Rev. Lett.* **1996**, *77*, 3865. (b) Perdew, J. P.; Burke, K.; Ernzerhof, M. *Phys. Rev. Lett.* **1997**, *78*, 1396.

(22) Adamo, C.; Barone, V. *J. Chem. Phys.* **1999**, *110*, 6158.

(23) (a) Barone, V.; Peralta, J. E.; Scuseria, G. E. *Nano Lett.* **2005**, *5*, 1830. (b) Bettinger, H. F. *J. Phys. Chem. B.* **2005**, *109*, 6922. (c) Ernzerhof, M.; Scuseria, G. *J. Chem. Phys.* **1999**, *110*, 5029. (d) Avramov, P. V.; Kudin, K. N.; Scuseria, G. E. *Chem. Phys. Lett.* **2003**, *370*, 597. (e) An, W.; Gao, Y.; Bulusu, S.; Zeng, X. C. *J. Chem. Phys.* **2005**, *122*, 204109. (f) Johansson, M. P.; Sundholm, D.; Vaara, J. *Angew. Chem., Int. Ed.* **2004**, *43*, 2678.

(24) Hay, P. J.; Wadt, W. R. *J. Chem. Phys.* **1985**, *82*, 270.

(25) (a) Reed, A. E.; Curtiss, L. A.; Weinhold, F. *Chem. Rev.* **1988**, *88*, 899. (b) Weinhold, F.; Landis, C. A. *Valency and Bonding: A Natural Bond Orbital Donor-Acceptor Perspective*; Cambridge University Press: Cambridge, 2005; p 760.

(26) Wiberg, K. *Tetrahedron* **1968**, *24*, 1083.

(27) http://www.chemcraftprog.com.

(28) Granovsky, A. A. http://lcc.chem.msu.ru/gran/gamess/index.html.

(29) Schmidt, M. W.; Baldridge, K. K.; Boatz, J. A.; Elbert, S. T.; Gordon, M. S.; Jensen, J. H.; Koseki, S.; Matsunaga, N.; Nguyen, K. A.; Su, S.; Windus, T. L.; Dupuis, M.; Montgomery, J. A. *J. Comput. Chem.* **1993**, *14*, 1347.

(30) Boys, S. F.; Bernardi, F. *Mol. Phys.* **1970**, *19*, 553.

(31) Dubicki, L.; Martin, R. L. *Inorg. Chem.* **1970**, *9*, 673.

(32) (a) Norman, J. G.; Kolari, H. J. *J. Am. Chem. Soc.* **1978**, *100*, 791. (b) Bursten, B. E.; Cotton, F. A. *Inorg. Chem.* **1981**, *20*, 3042.

(33) Nakatsuji, H.; Ushio, J.; Kanda, K.; Onishi, Y.; Kawamura, T.; Yonezawa, T. *Chem. Phys. Lett.* **1981**, *79*, 299.

(34) Cotton, F. A.; Dikarev, E. V.; Feng, X. *Inorg. Chim. Acta* **1995**, *237*, 19.

(35) Lichtenberger, D. L.; Pollard, J. R.; Lynn, M. A.; Cotton, F. A.; Feng, X. *J. Am. Chem. Soc.* **2000**, *122*, 3182.

(36) Wang, L.-L.; Johnson, D. D. *J. Phys. Chem. B* **2005**, *109*, 23113.

(37) Cotton, F. A.; Dikarev, E. V.; Petrukhina, M. A.; Stiriba, S.-E. *Organometallics* **2000**, *19*, 1402.

(38) Cotton, F. A.; Dikarev, E. V.; Petrukhina, M. A.; Taylor, R. E. *J. Am. Chem. Soc.* **2001**, *123*, 5831.

(39) Dikarev, E. V.; Li, B.; Rogachev, A. Yu.; Zhang, H.; Petrukhina, M. A. *Organometallics* **2008**, *27*, 3728.

(40) (a) Cotton, F. A.; Dikarev, E. V.; Petrukhina, M. A.; Stiriba, S.-E. *Polyhedron* **2000**, *19*, 1829. (b) Cotton, F. A.; Dikarev, E. V.; Petrukhina, M. A. *J. Am. Chem. Soc.* **2001**, *123*, 11655.

(41) Petrukhina, M. A.; Andreini, K. W.; Mack, J.; Scott, L. T. *J. Org. Chem.* **2005**, *70*, 5713.

(42) Filatov, A. S.; Rogachev, A. Yu.; Petrukhina, M. A. *Cryst. Growth Des.* **2006**, *6*, 1479.

(43) (a) Fagan, P. J.; Calabrese, J. C.; Malone, B. *Acc. Chem. Res.* **1992**, *25*, 134. (b) Balch, A.; Olmstead, M. M. *Chem. Rev.* **1998**, *98*, 2123. (c) Lee, K.; Song, H.; Park, J. T. *Acc. Chem. Rev.* **2003**, *36*, 78.

(44) Petrukhina, M. A.; Sevryugina, Y.; Rogachev, A. Yu.; Jackson, E. A.; Scott, L. T. *Angew. Chem., Int. Ed.* **2006**, *45*, 7208.

(45) Recent reviews:(a) Rabideau, P. W.; Sygula, A. *Acc. Chem. Res.* **1996**, *29*, 235. (b) Mehta, G.; Rao, H. S. P. *Tetrahedron* **1998**, *54*, 13325. (c) Wu, Y.-T.; Siegel, J. S. *Chem. Rev.* **2006**, *106*, 4843. (d) Tsefrikas, V. M.; Scott, L. T. *Chem. Rev.* **2006**, *106*, 4868.

(46) Elliott, E. L.; Hernandez, G. A.; Linden, A.; Siegel, J. S. *Org. Biomol. Chem.* **2005**, *3*, 407.

(47) Siegel, J. S.; Baldridge, K. K.; Linden, A.; Dorta, R. *J. Am. Chem. Soc.* **2006**, *128*, 10644.

(48) (a) Vecchi, P. A.; Alvarez, C. M.; Ellern, A.; Angelici, R. J.; Sygula, A.; Sygula, R.; Rabideau, P. W. *Angew. Chem., Int. Ed.* **2004**, *43*, 4497. (b) Vecchi, P. A.; Alvarez, C. M.; Ellern, A.; Angelici, R. J.; Sygula, A.; Sygula, R.; Rabideau, P. W. *Organometallics* **2005**, *24*, 4543. (c) Zhu, B.; Ellern, A.; Sygula, A.; Sygula, R; Angelici, R. J. *Organometallics* **2007**, *26*, 1721.

(49) (a) Petrukhina, M. A.; Scott, L. T. *Dalton Trans.* **2005**, 2969. (b) Petrukhina, M. A. *Angew. Chem., Int. Ed.* **2008**, *47*, 1550.

(50) Petrukhina, M. A.; Sevryugina, Y.; Rogachev, A. Yu.; Jackson, E. A.; Scott, L. T. *Organometallics* **2006**, *25*, 5492.

(51) The only *endo*-bound buckybowl complex was reported for sumanene. Amaya, T.; Sakane, H.; Hirao, T. *Angew. Chem., Int. Ed.* **2007**, *46*, 8376.

(52) Hirsch, A. *The Chemistry of Fullerenes*; Georg Thieme Verlag: Stuttgart, 1994.

(53) Rogachev, A. Yu.; Sevryugina, Y.; Filatov, A. S.; Petrukhina, M. A. *Dalton Trans.* **2007**, 3871.

JP901271G